We are IntechOpen,
the world's leading publisher of
Open Access books
Built by scientists, for scientists

6,900
Open access books available

185,000
International authors and editors

200M
Downloads

Our authors are among the

154
Countries delivered to

TOP 1%
most cited scientists

12.2%
Contributors from top 500 universities

BOOK CITATION INDEX
CLARIVATE ANALYTICS
INDEXED

WEB OF SCIENCE™

Selection of our books indexed in the Book Citation Index
in Web of Science™ Core Collection (BKCI)

Interested in publishing with us?
Contact book.department@intechopen.com

Numbers displayed above are based on latest data collected.
For more information visit www.intechopen.com

Tsunami Hazard Assessment for the Hokuriku Region, Japan: Toward Disaster Mitigation for Future Earthquakes

Michihiro Ohori, Yuri Masukawa and
Keisuke Kojima

Additional information is available at the end of the chapter

Abstract

In Japan, compared with the Pacific coast, the Japan Sea coast has low seismicity and has experienced very few occurrences of historical tsunami damage. These characteristics lead to some difficulties in the promotion of disaster prevention education, because the Japan Sea coast has not often been threatened by earthquakes and tsunamis. In our study, focusing on the Hokuriku region in Japan, we conducted a tsunami simulation and examined the resulting tsunami hazard map. Three potential faults of Mw7.6 earthquake were selected to generate the tsunami. In addition, we calculated these three events with Mw7.8, given the inherent uncertainty in source parameters. Aside from tsunami height, arrival time, inundation height, and inundation area, we calculated the seismic intensity and the liquefaction occurrence rate by simplified methods. Our results indicated that Suzu City in Ishikawa Prefecture, located in the northeastern part of the Noto Peninsula, has a relatively high potential risk of tsunami as well as strong motion and liquefaction. Thus, Suzu City would represent a highly appropriate area in which to promote disaster prevention education in the Hokuriku region.

Keywords: tsunami, simulation, hazard assessment, Hokuriku region, disaster mitigation

1. Introduction

The 2011 Tohoku earthquake (Mw9) generated a giant tsunami and caused the death of more than 18,000 inhabitants (including missing persons). Surprisingly, a considerable number of people did not evacuate due to a misunderstanding regarding the early-stage warning of a

3 m-high tsunami and/or too much trust in the protection afforded by high tidal banks, despite having sufficient evacuation time after the strong ground shaking. The Pacific coast of the Tohoku region has been repeatedly threatened by tsunamis, and thus appropriate disaster prevention education and evacuation drills have been conducted. However, it was neverthe-less surprising that there were such a high number of victims even in regions with high disaster prevention awareness.

Compared with the Pacific coast, the Japan Sea coast has experienced few tsunami disasters, especially in the Hokuriku region, where the seismicity is low; however, disaster prevention awareness is also low. To promote practical disaster prevention education by making full use of lessons learned from the tsunami disaster following the 2011 Tohoku earthquake, it is crucial to deepen our understanding of a devastating tsunami following strong ground shaking and relevant damage from an earthquake.

In this study, the focus of interest is the Hokuriku region (Fukui, Ishikawa, and Toyama Prefectures). To date, each prefecture has conducted its own tsunami simulation and published hazard maps in which the region is limited to its own prefecture [1–3]. When the same seismic fault is examined, source parameters differ between prefectures. Therefore, it is difficult to use hazard maps as teaching materials to gain an understanding of the whole picture of a tsunami disaster, as a tsunami obviously takes no account of administrative boundaries. In addition, cooperation between adjacent prefectures in the matter of preparedness for future tsunami disasters is not without problems.

The 2011 Tohoku earthquake (Mw9) prompted investigation on the possible occurrence of a tsunami on the Japan Sea coast in two different research projects: one by the Ministry of Land, Infrastructure and Transport [4] and the other by the Ministry of Education, Culture, Sports, Science and Technology [5]. However, since the coverage of these studies is very broad, and they do not specifically focus on the Hokuriku region, it may be difficult to make use of the project results in local disaster prevention education in our region of interest.

Here, we carried out hazard assessment of a tsunami following an earthquake in the Hokuriku region. After considering the whole region, we extracted a model district to be prioritized in future disaster education. Using a simplified method, ground shaking and liquefaction rates were evaluated to gain insight into tsunami hazard in relation to strong ground motion.

2. Analytical methods

2.1. Tsunami simulation

In the present study, we used TSUNAMI-K software, which was originally developed and published by a research group at Tohoku University as the analytical Fortran code of TUNAMI [6–8] and later incorporated with the GUI (graphical user interface) environment by Kozo Keikaku Engineering Inc. Details of the theory commentary are given in literatures [6–8]. The computer program TUNAMI developed by Tohoku University has been distributed worldwide

as part of the Tsunami Inundation Modeling Extension (TIME) project promoted by collaboration of the International Union of Geodesy and Geophysics (IUGG) and the Intergovernmental Oceanographic Commission (IOC) of the United Nations Educational, Scientific and Cultural Organization (UNESCO) during the International Decade for Natural Disaster Reduction (IDNDR). Currently it has been recognized as the UNESCO's standard evaluation method for tsunami and used by 36 institutions of 19 countries, which suffered or will suffer tsunami hazards. So, the accuracy and reliability of the code have been verified by many studies (e.g., [9–11]). Here, the outline of numerical calculations and the analytical conditions, implemented into the analytical codes, are briefly summarized.

2.1.1. Governing equations

For the tsunami analyses, the shallow-water long-wave theory is used. The governing equations are expressed in Eqs. (1)–(3).

$$\frac{\partial \eta}{\partial t} + \frac{\partial M}{\partial x} + \frac{\partial N}{\partial y} = 0 \tag{1}$$

$$\frac{\partial M}{\partial t} + \frac{\partial}{\partial x}\left(\frac{M^2}{D}\right) + \frac{\partial}{\partial y}\left(\frac{MN}{D}\right) + gD\frac{\partial \eta}{\partial x} + \frac{gn^2 M}{D^{7/3}}\sqrt{M^2 + N^2} = 0 \tag{2}$$

$$\frac{\partial N}{\partial t} + \frac{\partial}{\partial x}\left(\frac{MN}{D}\right) + \frac{\partial}{\partial y}\left(\frac{N^2}{D}\right) + gD\frac{\partial \eta}{\partial y} + \frac{gn^2 N}{D^{7/3}}\sqrt{M^2 + N^2} = 0 \tag{3}$$

Here, η is the water level, h is still water depth, D is the total water depth (h +η), g is the gravitational acceleration, n is Manning's roughness coefficient (described later), and M and N are the flow flux (flow rate per unit width) in the x- and y-direction, respectively. Eq. (1) represents a continuous equation, which corresponds to the law of conservation of mass. Eqs. (2) and (3) represent equations of motion for the x- and y-direction, respectively.

Eqs. (2) and (3) are derived from the Navier-Stokes equation, taking into account the characteristics of the tsunami: (a) the viscosity can be ignored since it is targeted for seawater, (b) the wavelength is long relative to the water depth, and (c) the seawater from the water surface to the sea bottom flows together at a uniform horizontal flow velocity. See Refs. [6–8] for detailed derivation.

Eqs. (2) and (3) are used when the tsunami height cannot be ignored with respect to the water depth in a shallow sea, usually at a water depth of 50 m (sometimes 100 m or 200 m). In the case of deep water, the second, third, and fifth terms of Eqs. (2) and (3) become small, and their solutions approach those from the linear long-wave equations. In the present study, Eqs. (2) and (3) are used as they are to calculate the tsunami inundation to the land.

2.1.2. Analytical range of seismic fault

Figure 1 shows the entire target area. The yellow frame in this figure represents the range for a detailed evaluation of the tsunami propagation. The coastal area of the western end
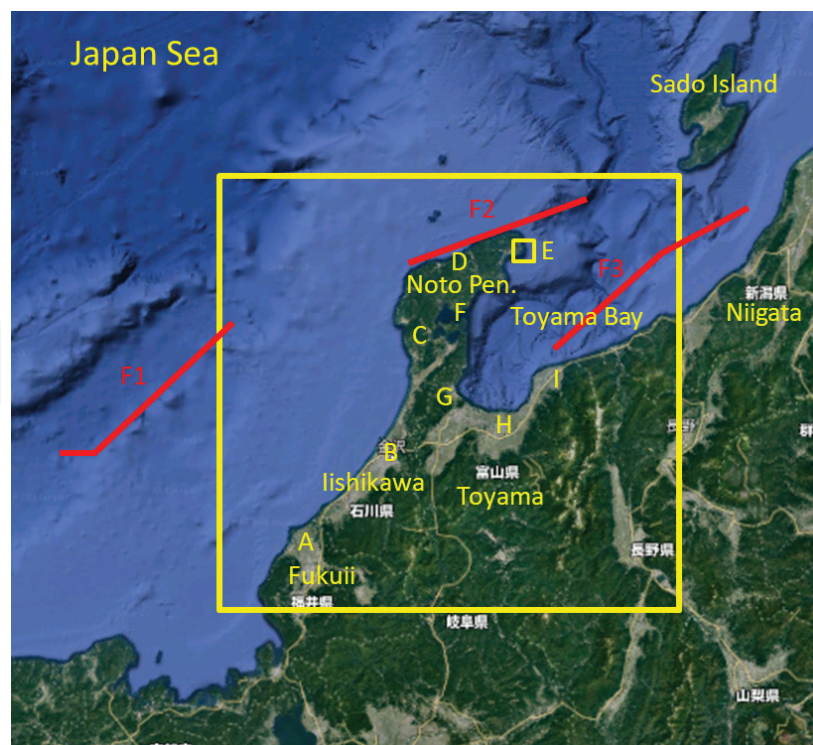
Figure 1. Map showing the entire target area. the range for a detailed evaluation of the tsunami propagation is denoted by the yellow frame. Surface projection of the three earthquake faults is denoted by a red line and labeled as F1–F3. Further explanation is described in the text. Main city locations discussed in the text labeled as A-G are Mikuni Town of Sakai City ("A"), Kanazawa City ("B"), Shiga Town ("C"), Wajima City ("D"), Suzu City ("E"), Anamizu Town ("F"), Himi City ("G"), Toyama City ("H"), and Nyuzen City ("I"). A small rectangle adjacent to "E" shows an area around Misaki Town of Suzu City illustrated in **Figures 11**, **12**. (Note that background map is from Google maps.)

(left) is Echizen Town, Fukui Prefecture, and that of the eastern end (right) is Itoigawa City, Niigata Prefecture (east of Toyama Prefecture). The seismic faults studied here are denoted by a red line in **Figure 1** and are (from the left) the Wakasa Sea Knoll Chain fault (labeled as F1), north off the Noto Peninsula fault (F2) and east off the Noto Peninsula fault (F3). Each of these three earthquake faults consists of two or three small faults with different strike angles.

2.1.3. Initial conditions

For the evaluation of crustal deformation of the seafloor accompanying the earthquake, we use the static deformation [12] of the sea bottom surface, which corresponds to the initial water level of the tsunami simulation. The fault parameters that specify the seismic fault model are set as shown in **Table 1**, referring to the report on the Ministry of Land, Infrastructure and Transport [4]. For each of the three seismic faults, two cases are calculated: Case 1 with Mw7.6 and Case 2 with Mw7.8 (in which slip displacement of the fault in Case 1 is doubled). Case 2 is intended to give inherent uncertainty in source parameters as a lesson from the 2011 Tohoku earthquake. In addition, it is assumed that the slip distribution on the fault plane is uniform and the propagation of rupture is not taken into account (the velocity of rupture propagation is assumed to be infinite).

Fault name	Segment No.	Depth* (km)	Strike angle (°)	Rake angle (°)	Slip angle (°)	Length (km)	Width (km)	Mw Case 1	Mw Case 2
Wakasa Sea-Knoll Chain	1	2.4	81	60	264	21.1	14.5	7.6	7.8
	2		47		145	36.3			
	3		54		215	29.9			
North-off Noto Pen.	1	1.1	64	45	113	48.3	19.7	7.6	7.8
	2		55		105	45.9			
East-off Noto Pen.	1	1.9	37	45	76	51.5	22.7	7.6	7.8
	2		55		102	34.1			

*'Depth' represents the upper end depth of the fault plane.

Table 1. Source parameters of earthquake faults in the present study.

2.1.4. Boundary conditions

2.1.4.1. Transmitting condition at offshore side

The method in Ref. [6] is used for the amount of outflow from the calculation area on the offshore side, in which free transmission is made and reflection to the calculation area is suppressed. It is assumed that the amount of water $\eta\,(g \times h)^{1/2}$ flows out at a progressive long-wave velocity of $(g \times h)^{1/2}$, where η is the wave level just inside the boundary.

2.1.4.2. Run-up condition to the land

To calculate the tsunami's run-up to land according to shallow-water long-wave theory, the method in Ref. [13] is used. In this method, the topography at the run-up fronts is treated as steplike grids, and the flow is evaluated using Eqs. (1)–(3). When the water level η of the seaside grid is higher than the ground height z of the landside grid, the difference is defined as the actual water depth D, and the water level and the flow rate are calculated. $D > 10^{-5}$ (m) is often used as a criterion for considering a tsunami's run-up to land (e.g., [14]). This kind of boundary to treat tsunami's run-up is called the moving boundary [8]. After comparison of several methods to treat the moving boundary, the method in Ref. [13] is selected and implemented into the computational code TUNAMI because of its accuracy [8].

2.1.4.3. Tide level conditions

The average sea level in the Japan Sea is 0.2 m higher than T. B. (mean sea level in Tokyo Bay). In the present study, the tide level is set to ±0 m.

2.1.5. Submarine topography data and land altitude data

For tsunami simulation, the seafloor depth data and land altitude data are required. For the offshore, we use the 1 km grid water depth data of the Japan Sea area from JTOPO30 (30-s grid

water depth data in Japan's coastal waters) [15] published by the Marine Information Research Center of the Japan Hydrographic Association. For the nearshore, we use the coastal 500 m grid water depth data [16] published by the Japan Coast Guard. Furthermore, for the land data necessary for the run-up analysis, we use the 50 m grid land altitude data [17] published by the Geospatial Information Authority of Japan.

2.1.6. Numerical scheme

For numerical calculations, Eqs. (1)–(3) are discretized and solved by using the finite difference method. An orthogonal coordinate grid is used in the spatial domain, and a staggered grid is used in the variable placement. The leapfrog method is used in the time domain, which provides neutral stability with no dissipation error. In the discretization of the spatial domain, three grid sizes are used: 450 m for the whole region, 150 m for the intermediate region, and 50 m for the nearshore and the land. The whole region for analysis is shown in **Figure 1**, in which the yellow frame is the region discretized into 50 m grids. We analyze the calculations performed in the time domain with a time step of 0.1 s and tsunami propagation for 180 min after an earthquake fault ruptures.

2.1.7. Manning's roughness

The fifth term in Eqs. (2) and (3) represents the friction effect against the sea bottom during tsunami propagation, which varies rapidly when Manning's roughness n changes. In the present study, n is fixed at 0.025, with a reference to [10].

2.2. Evaluation of strong motion

To provide an overview of a disaster not only from the perspective of tsunami inundation but also from the damage occurrence of strong ground shaking and liquefaction, simplified methods based on the attenuation formula of the maximum velocity are used to calculate the seismic intensity and the liquefaction occurrence rate in the whole region. Here, the methodologies are briefly summarized.

2.2.1. Seismic intensity

The seismic intensity (The Japan Meteorological Agency seismic intensity scale) is evaluated through three steps: (1) the evaluation of the maximum velocity on the engineering bedrock, (2) the evaluation of the amplification factor of the maximum velocity from the engineering bedrock to the ground surface, and (3) the evaluation of the seismic intensity from the maximum velocity at the surface.

In the first step, the maximum velocity on the engineering bedrock (a layer with the S-wave velocity of 600 (m/s)) is evaluated using Eq. (4) by the empirical formula [18–19]:

$$log_{10} PGV_{600} = 0.58 M_w + 0.0038D + d - 1.29 - log_{10} \left(X + 0.0028 \times 10^{0.50M_w} \right) - 0.002X \quad (4)$$

where PGV is abbreviation of "peak ground velocity", PGV_{600} is the maximum velocity (cm/s) on the engineering bedrock with S-wave velocity of 600 m/s, Mw is the moment magnitude, D

is the depth of the source (km), d is the coefficient depending on the earthquake type (d = 0 for a crustal earthquake, d = −0.02 for an interplate earthquake, and d = 0.12 for an in-plate earthquake), and X is the fault's shortest distance between the fault plane and the target site (km). In the present study, the maximum velocity is estimated for a crustal earthquake. Eq. (4) is obtained by the regression analysis based on 543 data of the maximum velocity from 21 earthquakes that occurred in Japan (Mw5.8–8.2). Its validity and usefulness have been confirmed by many researchers in many earthquakes (e.g., [20–24]).

In the second step, the amplification factor of the maximum velocity from the engineering bedrock to the surface is calculated by the following relationship [25]:

$$log_{10} \, ARV = -0.852 \; log_{10} \, (AVS30/600) \tag{5}$$

where ARV (m/s) represents the amplification rate factor of the maximum velocity from the engineering bedrock to the surface and AVS30 (m/s) represents the average S-wave velocity from the surface to a depth of 30 m, ranging between 100 and 1500 m/s. According to Eq. (5), the ground motion becomes larger when AVS30 is lower than 600 m/s, whereas it becomes smaller when AVS30 is higher than 600 m/s. The maximum velocity at the ground surface, PGV, can be obtained by multiplying the maximum velocity at the engineering velocity, PGV_{600}, in Eq. (4) by the amplification factor ARV in Eq. (5):

$$\begin{aligned} log_{10} \, PGVs &= log_{10} \, (PGV_{600} \times ARV) = log_{10} \, PGV_{600} + log_{10} \, ARV \\ &= log_{10} \, PGV_{600} - 0.852 \; log_{10} \, (AVS30/600) \end{aligned} \tag{6}$$

In the third step, according to Refs. [26, 27], the seismic intensity on the ground surface can be calculated using the following formula:

$$I = 2.286 + 2.088 \times log_{10} \, PGVs \tag{7}$$

Using the above three-step procedure, it is possible to calculate the seismic intensity at an arbitrary point from a given seismic fault. In the present study, using the AVS30 of a 250 m grid based on the geomorphologic classification published by NIED's Japan Seismic Hazard Information Station (J-SHIS) [28, 29], the seismic intensity of the targeted area is evaluated.

2.2.2. Liquefaction occurrence rate

The relationship between the seismic intensity and the liquefaction occurrence rate [30, 31] is expressed as:

$$P_{liq}(I) = \Phi\big((I - \mu)/\sigma\big) \tag{8}$$

where $P_{liq}(I)$ represents the liquefaction occurrence rate at the seismic intensity I, Φ is the cumulative normal distribution function, μ is the mean value, and σ is the standard deviation; μ and σ are determined by classifying 15 types of geomorphologic classification—representing the potential to liquefy—into 4 groups according to liquefaction risk and by performing a regression analysis for each group with the least squares method based on the data of seismic intensity and liquefaction occurrence rate (see Refs. [30, 31] for details). Parameters to evaluate

Group	Geomorphologic classification liable to liquefy	μ	σ
1	Natural levee, abandoned river channel, lower slopes of dune, lowland between coastal dunes and bars, reclaimed land, filled land	6.960	0.761
2	Alluvial fan, alluvial fan with slope angle of less than 1/100, marine sand, and gravel bars	7.160	0.773
3	Back marsh, delta and coastal lowland, sand dune	7.906	0.933
4	Gravelly terrace, valley bottom lowland, valley bottom lowland with slope angle of less than 1/100	7.231	0.628

Table 2. Parameter to evaluate the liquefaction occurrence rate from Refs. [30, 31].

the liquefaction occurrence rate, μ and σ, are summarized in **Table 2**. For example, liquefaction begins to occur near seismic intensity 5.0. in group 1, which is the most liable to liquefy (natural levees, abandoned river channels, lower slopes of dunes, lowland between coastal dunes and bars, reclaimed land, and filled land). Note that parameters μ and σ in **Table 2** are determined based on the liquefaction data over 1400 from the recent 9 damaging earthquakes in Japan [30, 31] and applied to successfully reproduce the liquefaction occurrence locations due to the 2011 Tohoku earthquake [32].

3. Results

3.1. Overview of tsunami propagation

For each of the three earthquake faults, we conducted a tsunami simulation on two cases with different magnitudes: Case 1 Mw7.6 and Case 2 Mw7.8. The maximum tsunami height is shown in **Figures 2–7**. The displayed range of these figures corresponds to the yellow frame inside **Figure 1**, with the southwestern end as the origin, the distance in the east-west and north-south direction (km) is taken in the horizontal direction, and the maximum tsunami
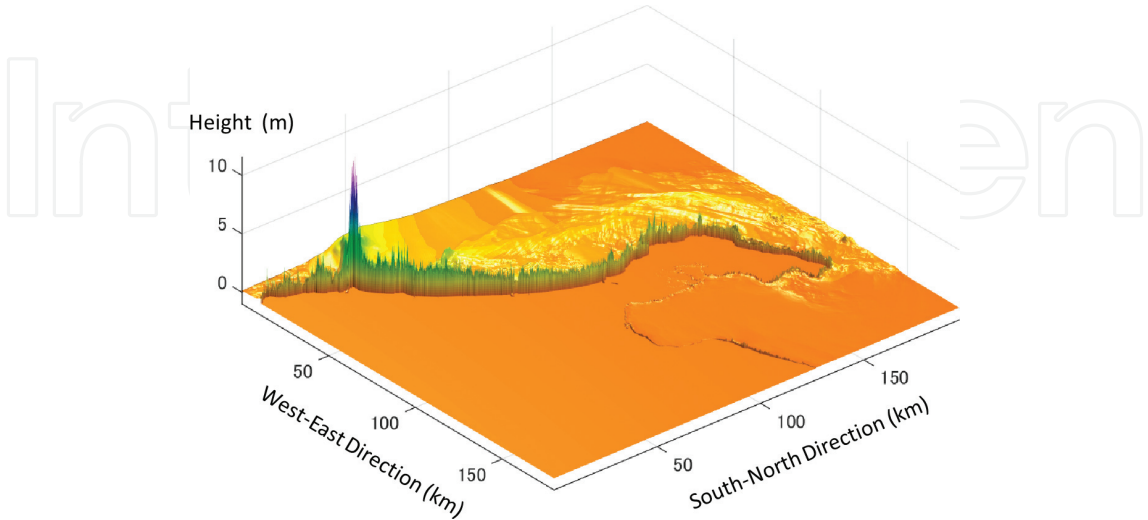

Figure 2. Map showing the maximum tsunami height for Case 1 (Mw7.6) of the Wakasa Sea knoll chain fault. The displaying range corresponds to the yellow frame inside **Figure 1**.

height is taken in the vertical direction (m). Similar plots have been done for the inundation depth and tsunami arrival time but omitted because of space. The general features from these results are discussed below.

3.1.1. Wakasa Sea knoll chain fault

The tsunami height in Case 1 (Mw7.6) (**Figure 2**) reaches a maximum of 9.0 m in Sakai City (Mikuni Town), Fukui Prefecture; ∼2.0 m in the vicinity of Kanazawa City, Ishikawa Prefecture; 0.5–2.0 m on the western side of the Noto Peninsula; and ∼0.1 cm in the coastal area of Toyama Prefecture. The spatial distribution characteristics of the inundation depth of the tsunami are similar to those of the tsunami height. Many areas are flooded from Fukui Prefecture to the western coast of the Noto Peninsula in Ishikawa Prefecture. The maximum inundation depth reaches 8.5 m in Sakai City (Mikuni Town), Fukui Prefecture.

The tsunami height in Case 2 (Mw7.8) (**Figure 3**) reaches a maximum of 13 m in Sakai City (Mikuni Town) in Fukui Prefecture; ∼4.0 m in the coastal area around Kanazawa City, Ishikawa Prefecture; 3.1 m in Hakui City, Ishikawa Prefecture; 0.3 m in Himi City, Toyama Prefecture; and ∼0.2 m in Toyama City, Toyama Prefecture. As for the inundation of the tsunami, many areas are flooded from Fukui Prefecture to the northern Noto Peninsula in Ishikawa Prefecture. The maximum inundation depth reaches 12 m in Mikuni Town in Sakai City, Fukui Prefecture.

Since the Wakasa Sea Knoll Chain fault is located offshore compared with the other two faults, the arrival time of the tsunami is prolonged. In the vicinity of Sakai City (Mikuni Town), Fukui Prefecture, where the maximum tsunami height occurs, the arrival time is ∼29 min from the occurrence of the earthquake. On the western coast of the Noto Peninsula in Ishikawa Prefecture, it is 29–37 min.
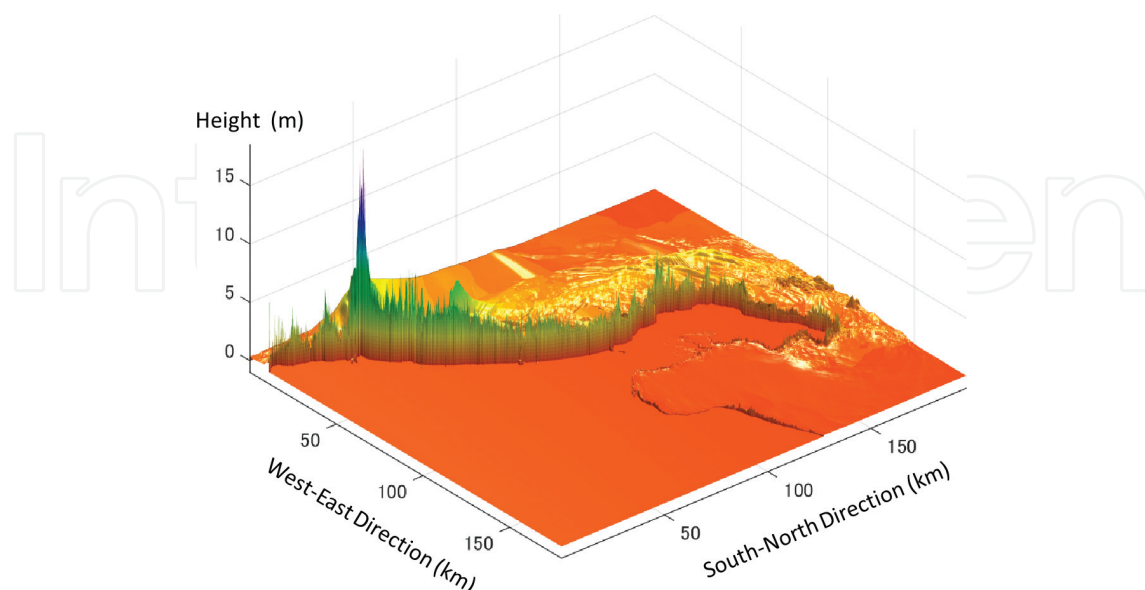

Figure 3. Map showing the maximum tsunami height for Case 2 (Mw7.8) of the Wakasa Sea knoll chain fault. Other conditions are the same as in **Figure 2**.

3.1.2. North off the Noto Peninsula fault

The maximum height of the tsunami in Case 1 (Mw7.6) (**Figure 4**) occurs in Suzu City, Ishikawa Prefecture, reaching 7.1 m. It is 1.0–3.5 m in the northern Noto Peninsula near the earthquake fault, 0.5–2.0 m in Toyama prefecture, 1.0–2.0 m in the coastal area around Kanazawa City, and 0.5–1.0 m in Sakai City (Mikuni Town) in Fukui Prefecture. The inundation depth of the tsunami is similar to that of the tsunami height. Many areas are flooded from the northeastern tip of the Noto Peninsula to its western coast. The maximum inundation depth reaches ∼4.0 m on the eastern coast of Suzu City, Ishikawa Prefecture (around Horyu Town), 1.0–3.0 m on the western coast, and 1.0–4.0 m in Wajima City (around Wajima Port).

The maximum height of the tsunami height in Case 2 (Mw7.8) (**Figure 5**) occurs in Suzu City, Ishikawa Prefecture, reaching 9.6 m. It is 3.0–6.0 m in the northern side of Noto Peninsula;
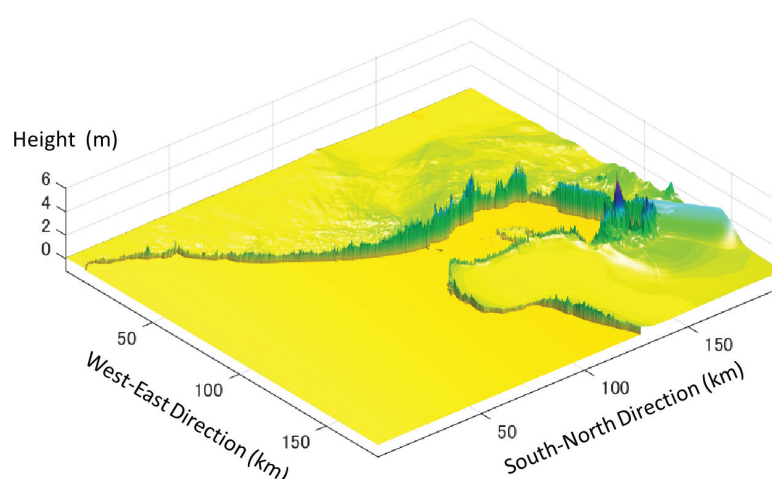

Figure 4. Map showing the maximum tsunami height for Case 1 (Mw7.6) of the north off the Noto Peninsula fault. Other conditions are the same as in **Figure 2**.
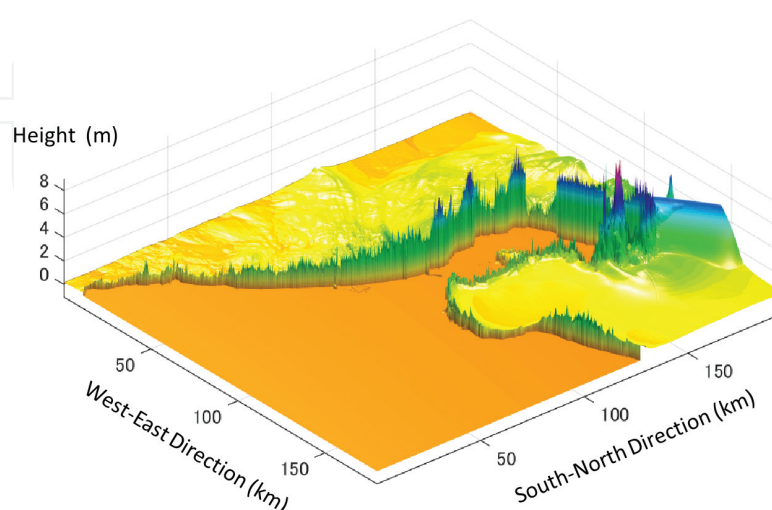

Figure 5. Map showing the maximum tsunami height for Case 2 (Mw7.8) of the north off the Noto Peninsula fault. Other conditions are the same as in **Figure 2**.

1.0–3.0 m in Toyama Prefecture; 2.0 m in the coastal area around Kanazawa City; and 1.5 m in Sakai City (Mikuni Town), Fukui Prefecture. The inundation depth of the tsunami has distribution characteristics similar to the tsunami height. Many areas are flooded from the northeastern tip of the Noto Peninsula to its western coast. The maximum inundation depth
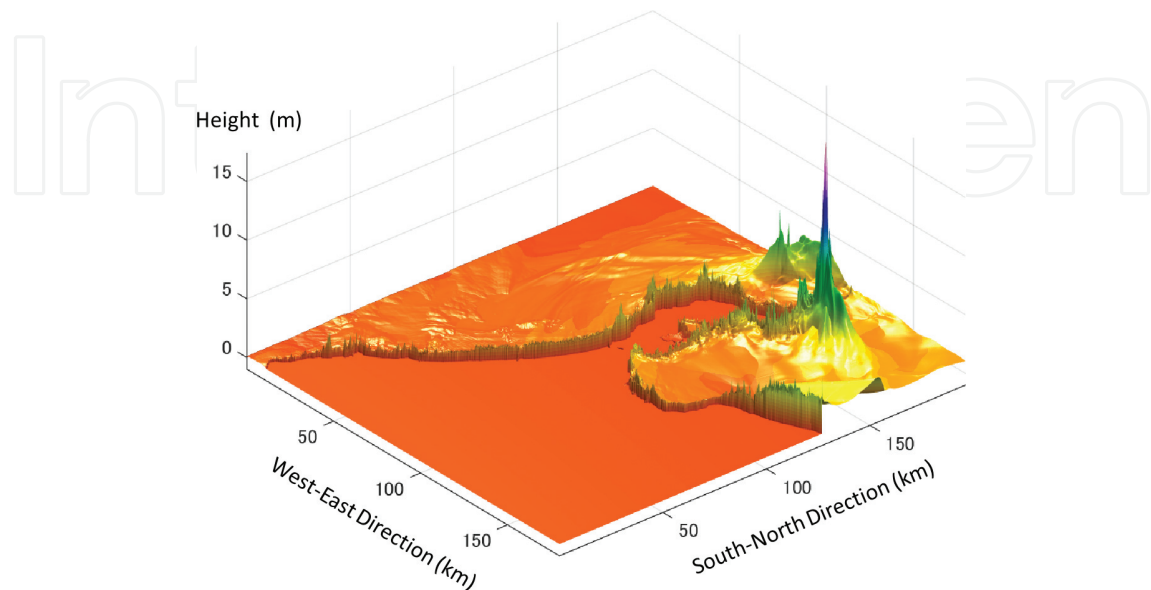

Figure 6. Map showing the maximum tsunami height for Case 1 (Mw7.6) of the east off the Noto Peninsula fault. Other conditions are the same as in **Figure 2**.
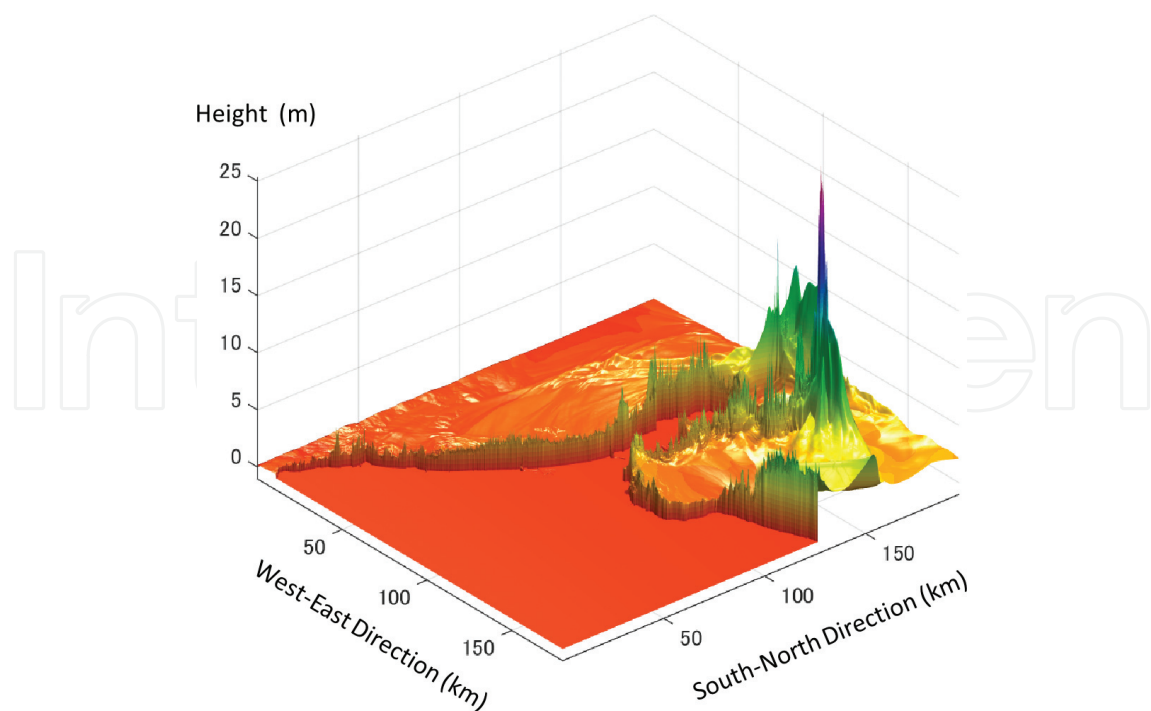

Figure 7. Map showing the maximum tsunami height for Case 2 (Mw7.8) of the east off the Noto Peninsula fault. Other conditions are the same as in **Figure 2**.

reaches 7.0 m in Suzu City (around Horyu Town). In addition, other areas of Suzu City, Wajima City (around Wajima Port), and Shiga Town (around the Togi river mouth) have an inundation depth of 1.0–4.0 m.

North off the Noto Peninsula fault is close to the land area, and the tsunami arrives within 3 min at its fastest. Going around the Noto Peninsula, the tsunami takes 12 min to Suzu City, Ishikawa Prefecture. It reaches the prefectural border between Toyama and Niigata Prefectures in ∼15 min and arrives in Fukui Prefecture in 100 min.

3.1.3. East off the Noto Peninsula fault

The tsunami height in Case 1 (Mw 7.6) (**Figure 6**) reaches a maximum of 13.8 m in Suzu City (Kodomari), Ishikawa Prefecture; 6.0–8.0 m in the vicinity of the prefectural border between Toyama and Niigata Prefectures; ∼2.5 m in the coastal area around Toyama City; ∼2.0 m in the coastal area near Kanazawa City; and 1.0–2.5 m in Sakai City (Mikuni Town), Fukui Prefecture. The spatial distribution characteristics of the inundation depth of the tsunami are similar to those of the tsunami height. The maximum inundation depth reaches ∼12.0 m in Suzu City (around Misaki Town). It is 1.0–7.0 m in other coastal areas of Suzu City and 1 m in Himi City, Toyama Prefecture (around Himi Fishing Port).

The maximum height of the tsunami in Case 2 (Mw 7.8) (**Figure 7**) is 21.4 m in Suzu City, Ishikawa Prefecture. It reaches 6.5 m in Anamizu Town, Ishikawa Prefecture; 3.0–6.0 m on the northern side of the Noto Peninsula; 2.0–3.0 m in the coastal area around Toyama City; ∼7.5 m in the vicinity of the prefectures border between Toyama and Niigata prefectures; 2.0 m in the coastal area around Kanazawa City; and 1.0–2.0 m around Sakai City (Mikuni Town), Fukui Prefecture. The inundation depth of the tsunami shows distribution characteristics similar to those of the tsunami height. Many areas are flooded from the northeastern tip of the Noto Peninsula to the coast of Toyama Bay. The maximum inundation depth reaches about 20 m in Suzu City (around Misaki Town) and is 1.0–3.0 m in Himi City, Toyama Prefecture (around Himi Fishing Port).

East off the Noto Peninsula fault is also close to the land area, and the tsunami arrives within 3 min at its fastest. The arrival time is ∼6 min near the prefectures border between Niigata and Toyama prefectures, ∼8 min in Sado Island, and 12 min in Suzu City, Ishikawa Prefecture. It takes about 105 min to arrive in the vicinity of Kanazawa City, Ishikawa Prefecture, and 135 min in Sakai City (Mikuni Town) in Fukui Prefecture.

3.1.4. Other findings

In Case 2, the slip displacement on the fault is double that of Case 1, meaning that the tsunami height is nearly double in the vicinity of the fault, although in the coastal area away from the fault the height is ∼1.5 times. In this analysis, the nonlinear long-wave equations are solved for the whole area, and in the coastal area near the land, the water becomes shallow and the effect of the submarine friction term increases.

The overall distribution characteristics of tsunami height change significantly for each of the three faults; except in the vicinity of the fault, the tsunami height at the Noto Peninsula tends to be high. In particular, it is predicted that Suzu City, Ishikawa Prefecture, located at the tip of the Noto Peninsula, has a high tsunami and broad inundation areas compared with other areas.
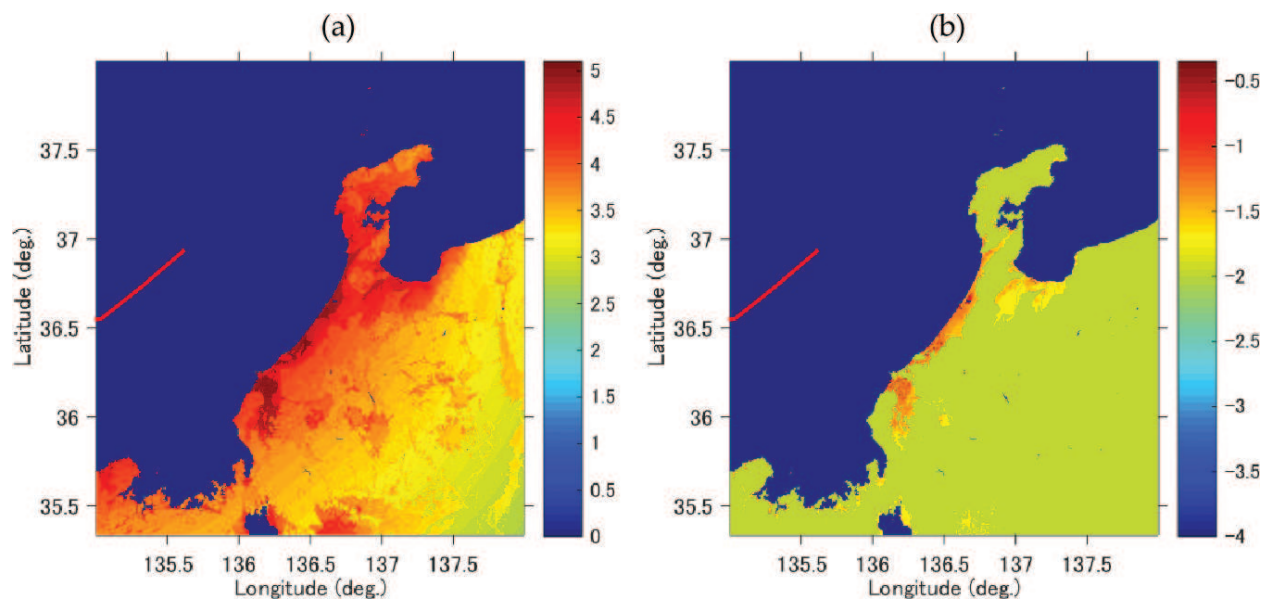

Figure 8. Map showing the seismic intensity (a) and the liquefaction occurrence rate (b) for Case 1 (Mw7.6) of the Wakasa Sea knoll chain fault. Note that color chart for the liquefaction occurrence rate (%) is expressed in log scale.
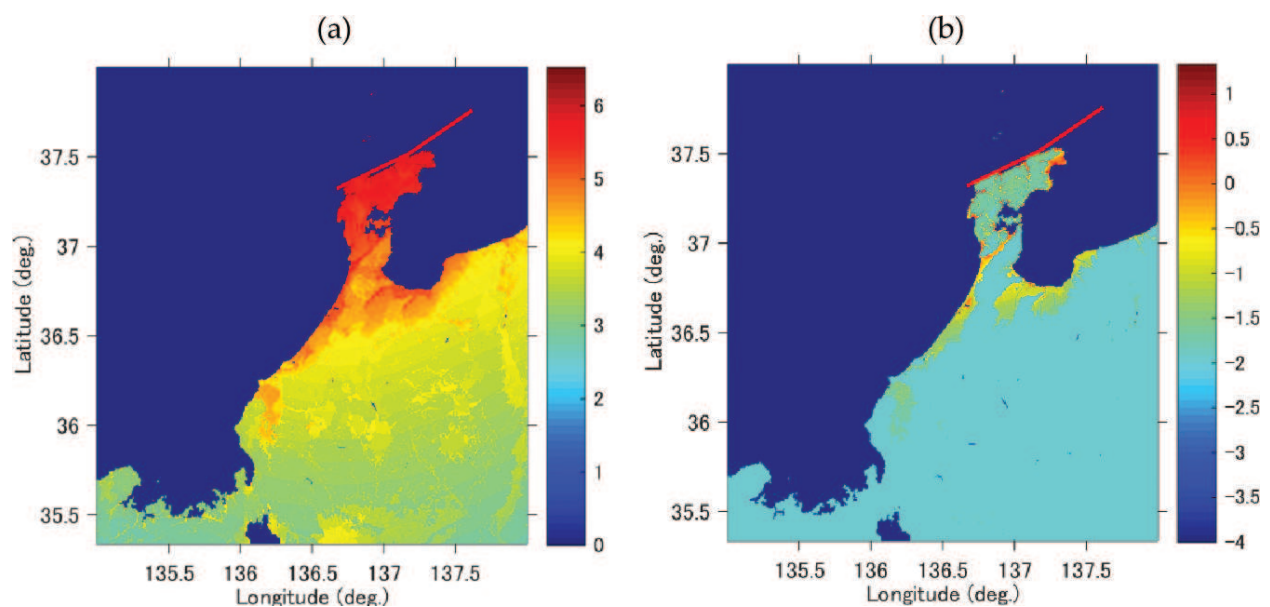

Figure 9. Map showing the seismic intensity (a) and the liquefaction occurrence rate (b) for Case 1 (Mw7.6) of the north off the Noto Peninsula fault. Other conditions are the same as in **Figure 8**.
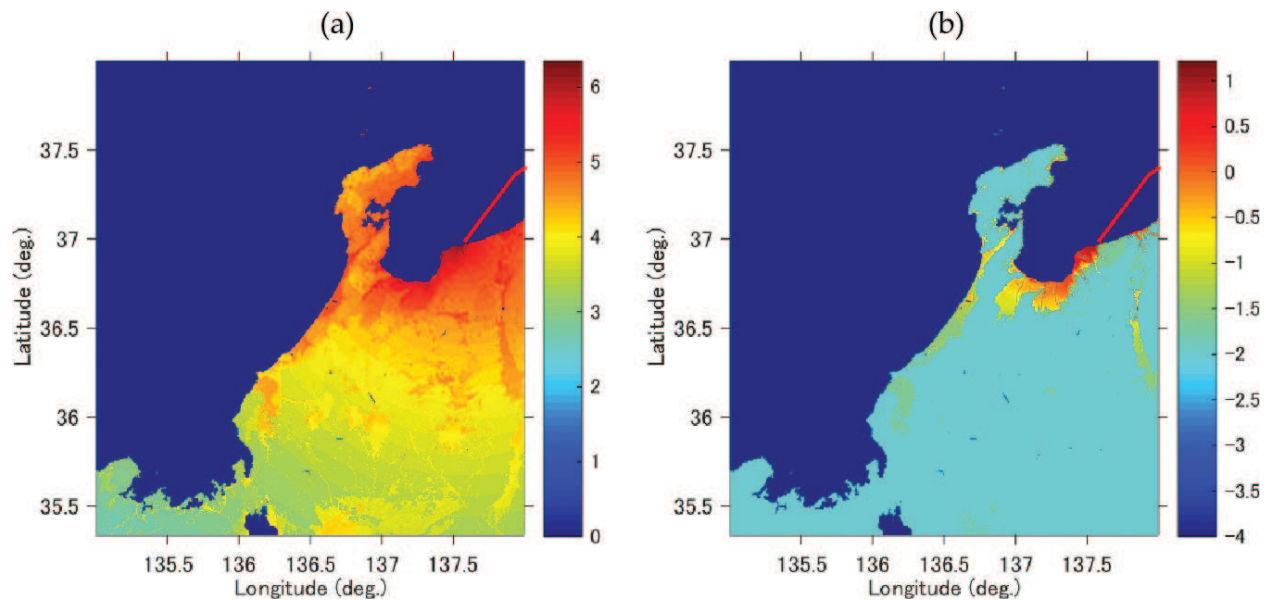
Figure 10. Map showing the seismic intensity (a) and the liquefaction occurrence rate (b) for Case 1 (Mw7.6) of the east off the Noto Peninsula fault. Other conditions are the same as in **Figure 8**.

3.2. From the perspective of strong ground motion

For a better understanding of a tsunami in a series of disasters triggered by an earthquake, the ground shaking and liquefaction occurrence rates were calculated for each fault. The seismic intensity and the liquefaction occurrence rate depend on the maximum velocity evaluated by Eq. (4). As can be seen from this equation, the difference of 0.2 in Mw between Cases 1 and 2 leads to a difference of 5–25% in the maximum velocity, depending on the fault distance. It also leads to a difference of 0.04–0.2 in the seismic intensity. These differences become smaller when the site is closer to the epicenter. Therefore, for the seismic intensity and liquefaction occurrence rate, here the results only for Case 1 are shown and discussed.

The maximum seismic intensity across the whole range is 5+ for the Wakasa Sea Knoll Chain fault (**Figure 8(a)**), 6+ for north off the Noto Peninsula fault (**Figure 9(a)**), and 6+ for east off the Noto Peninsula fault (**Figure 10(a)**). The maximum liquefaction occurrence rate across the whole range is 0.45% for the Wakasa Sea Knoll Chain fault (**Figure 8(b)**), 21% for north off the Noto Peninsula fault (**Figure 9(b)**), and 16% for east off the Noto Peninsula fault (**Figure 10(b)**).

4. Discussion

Calculation of the inundation area in the target area using a geographic information system (GIS) showed that the largest inundation area was estimated to be about 38 km^2 in Case 2 east off the Noto Peninsula fault, followed by ~17 km^2 in Case 2 north off the Noto Peninsula fault. In Case 2 of the Wakasa Sea Knoll Chain fault, the inundation area was ~7.6 km^2, which is slightly smaller

than the area of $\sim$9.0 km^2 in Case 1 east off the Noto Peninsula fault. Comparing Case 2 with Case 1, the inundation area increased 2.2 times in the Wakasa Sea Knoll Chain fault and 2.9 times north off the Noto Peninsula fault, 4.2 times east off the Noto Peninsula fault. In Case 2, the slip displacement on the fault is double that of Case 1, but the inundation area of the tsunami is much greater than that.

After observing the inundation area using the GIS, we decided to focus on Suzu City, Ishikawa Prefecture, which is expected to have the largest inundation area from both north off the Noto Peninsula fault and east off the Noto Peninsula fault. As an example, the inundation area of the city from the east off the Noto Peninsula fault is illustrated in **Figures 11** and **12**, which highlight the area around Misaki Town, Suzu City. In Case 2 (**Figure 12**), the tsunami runs up $\sim$1.9 km from the mouth of the Kino River, which is 1.5 times further than in Case 1 (**Figure 11**). In other inundation areas of the city, the tsunami runs up 1.5–1.7 km further from the coast in Case 2, which is two to four times the distance in Case 1. The inundation area of Suzu City from east off the Noto Peninsula fault is $\sim$5.3 km^2 in Case 1, and $\sim$17.4 km^2 in Case 2, which is $\sim$3.3 times larger. The inundation area of Suzu City from north off the Noto Peninsula fault is $\sim$2.3 km^2 in Case 1, and $\sim$7.4 km^2 in Case 2, which is $\sim$3.2 times larger (the figures are omitted due to space constraints).

Next, for the tip of the Noto Peninsula including Suzu City in Ishikawa Prefecture, an enlarged map of the seismic intensity and the liquefaction occurrence rate for north off the Noto Peninsula fault and east off the Noto Peninsula fault is shown in **Figures 13** and **14**. The lowland along the coast of Suzu City is subjected to strong shaking, with the seismic intensity
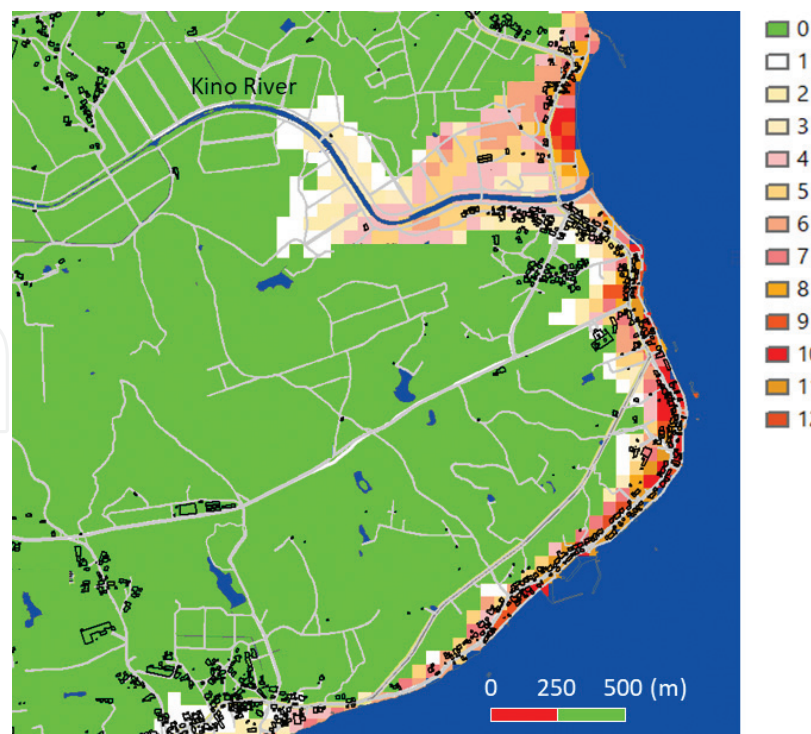

Figure 11. Enlarged map showing the inundation area (around Misaki Town) of Suzu City for Case 1 (Mw7.6) of the east off the Noto Peninsula fault. Note that color chart shows the inundation height (m).
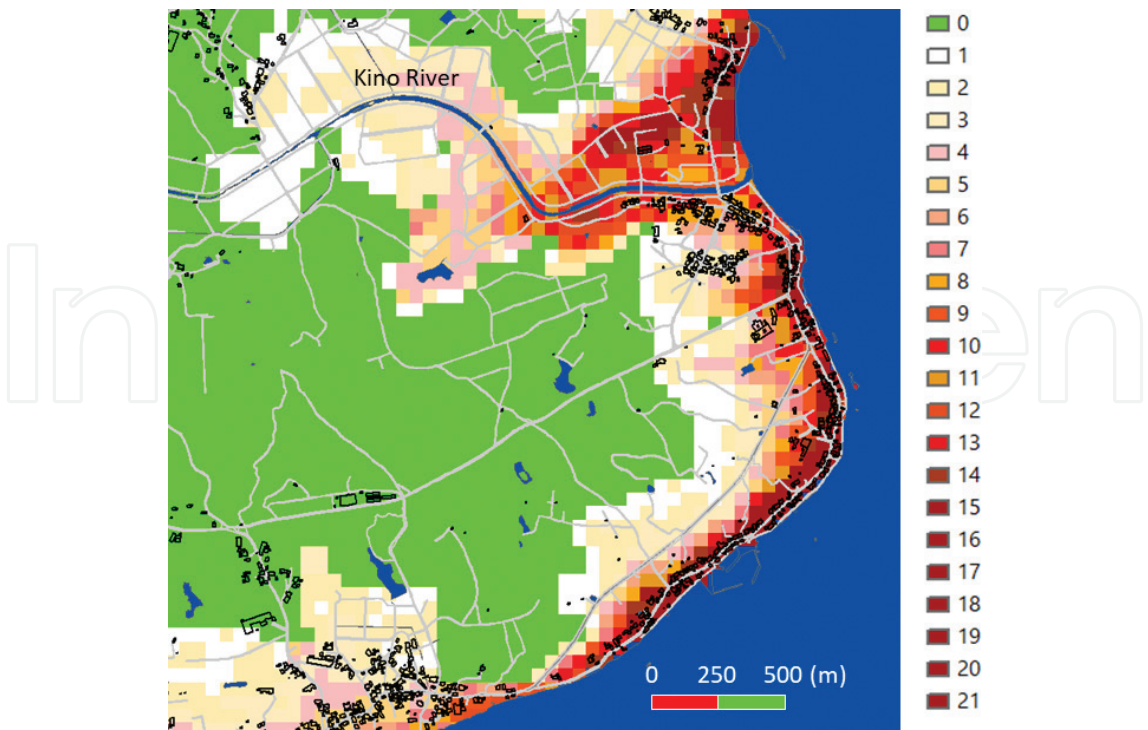
Figure 12. Enlarged map showing the inundation area (around Misaki Town) of Suzu City for Case 2 (Mw7.8) of the east off the Noto Peninsula fault. Other conditions are the same as in **Figure 11**.
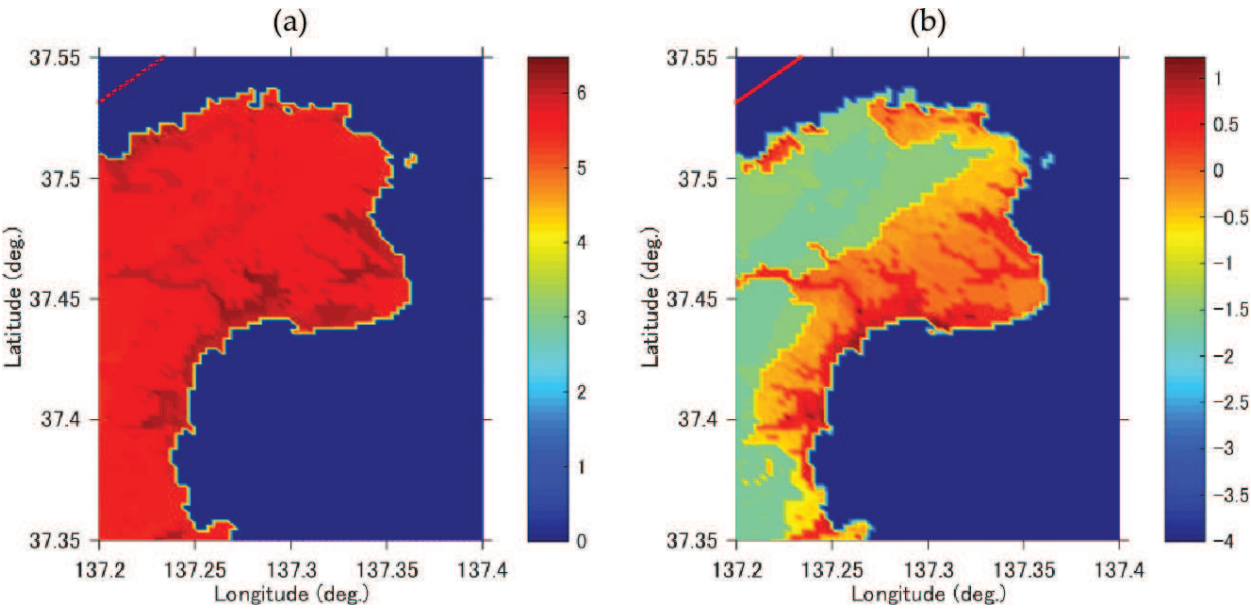

Figure 13. Enlarged map around the tip of the Noto Peninsula including Suzu City showing the seismic intensity (a) and the liquefaction occurrence rate (b) for Case 1 (Mw7.6) of the north off the Noto peninsula fault. Other conditions are the same as in **Figure 8**.
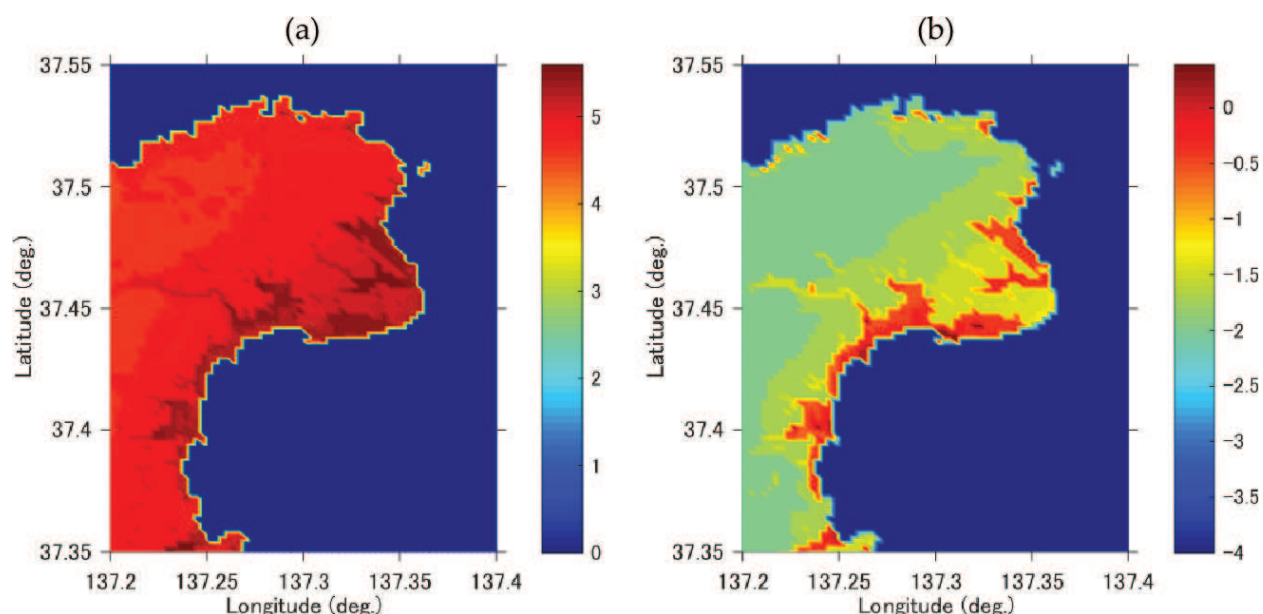
Figure 14. Enlarged map around Suzu City showing the seismic intensity (a) and the liquefaction occurrence rate (b) for Case 1 (Mw7.6) of the east off the Noto Peninsula fault. Other conditions are the same as in **Figure 8**.

reaching 6+ for the north off the Noto Peninsula fault and 6– for the east off the Noto Peninsula fault. Their liquefaction occurrence rate reaches 16 and 2.4%, respectively.

The inundation area of a tsunami is likely to occur in the coastal lowland, where strong ground motion may induce building damage and soil liquefaction. Therefore, it is important to examine the impact of damage caused by ground shaking on evacuation route and evacuation time. This is not limited to Suzu City but is common to the entire area where there is flooding caused by the tsunami and provides an important perspective for future damage estimation.

As noted, in the Hokuriku region, relatively few earthquakes are felt, and disaster prevention awareness is low. The resources (people, time, budget, etc.) that can be input for the promotion of disaster education are always limited. Under these circumstances, to obtain the maximum effect from limited resources, it is preferable to introduce intensive resources in a specific area with a high disaster risk, rather than treating the whole area equally. In this respect, Suzu City may be a model district, and if the promotion of disaster prevention is successful in the city, it could be fruitfully expanded to other areas.

5. Conclusions

In our study, focusing on the Hokuriku region in Japan, we conducted a tsunami simulation and examined the resulting tsunami hazard map. Three potential faults of Mw7.6 earthquake were selected to generate the tsunami: the Wakasa Sea Knoll Chain fault, north off the Noto Peninsula fault, and east off the Noto Peninsula fault. In addition, we calculated these three

events with Mw7.8, given the inherent uncertainty in source parameters. Aside from tsunami height, arrival time, inundation height, and inundation area, we calculated the seismic intensity and the liquefaction occurrence rate by simplified methods. Our findings in the present study are summarized as follows.

- In Case 2 (Mw7.8), the slip displacement on the fault is double that of Case 1 (Mw7.6), meaning that the tsunami height is nearly double in the vicinity of the fault, although in the coastal area away from the fault the tsunami height is ~1.5 times. In this analysis, the nonlinear long-wave equations are solved for the whole region, and in the coastal area near the land, the water becomes shallow and the effect of the submarine friction term increases.

- Comparing Case 2 with Case 1, the inundation area increased 2.2 times in the Wakasa Sea Knoll Chain fault and 2.9 times north off the Noto Peninsula fault, 4.2 times east off the Noto Peninsula fault. In Case 2, the slip displacement on the fault is double that of Case 1, but the inundation area of the tsunami is much greater than that.

- The overall distribution characteristics of tsunami height change significantly for each of the three faults; except in the vicinity of the fault, the tsunami height at the Noto Peninsula tends to be high. In particular, it is predicted that Suzu City, Ishikawa Prefecture, located at the tip of the Noto Peninsula, has a high tsunami and broad inundation areas compared with other areas.

- Our results indicated that Suzu City in Ishikawa Prefecture, located in the northeastern part of the Noto Peninsula, has a relatively high potential risk of tsunami as well as strong motion and liquefaction. Thus, Suzu City would represent a highly appropriate area in which to promote disaster prevention education in the Hokuriku region.

- The inundation area of a tsunami is likely to occur in the coastal lowland, where strong ground motion may induce building damage and soil liquefaction. Therefore, it is important to examine the impact of damage caused by ground shaking on evacuation route and evacuation time. This is not limited to Suzu City but is common to the entire area where there is flooding caused by the tsunami and provides an important perspective for future damage estimation.

Acknowledgements

Author details

Michihiro Ohori[1]*, Yuri Masukawa[2,3] and Keisuke Kojima[4]

*Address all correspondence to: ohorim@u-fukui.ac.jp

1 Research Institute of Nuclear Engineering, University of Fukui, Tsuruga, Japan

2 Graduate School, University of Fukui, Fukui, Japan

3 CTI Engineering Co., Ltd., Japan

4 Department of Architecture and Civil Engineering, University of Fukui, Fukui, Japan

References

[1] Fukui Prefecture. The Tsunami Simulation Results in Fukui Prefecture http://www.pref.fukui.lg.jp/doc/kikitaisaku/kikitaisaku/tunami-soutei.html (in Japanese, last accessed in April 30, 2018)

[2] Ishikawa Prefecture. The Tsunami Hazard Map in Ishikawa Prefecture http://www.pref.ishikawa.lg.jp/bousai/kikikanri_g/tsunami_info.htm (in Japanese, last accessed in April 30, 2018)

[3] Toyama Prefecture. The Outline of the Results of the Tsunami Simulation Survey http://www.pref.toyama.jp/cms_pfile/00017580/01067018.pdf (in Japanese, last accessed in April 30, 2018)

[4] Ministry of Land, Infrastructure and Transport, Study Group on Large Earthquakes in the Japan Sea, Report on the Study Group on Large Earthquakes in the Japan Sea. September, 2014 http://www.mlit.go.jp/river/shinngikai_blog/daikibojishinchousa/ (in Japanese, last accessed in April 30, 2018)

[5] Ministry of Education, Culture, Sports, Science and Technology. Japan Sea Earthquake and Tsunami Research Project http://www.eri.u-tokyo.ac.jp/project/Japan_Sea/index.html (in Japanese, last accessed in April 30, 2018)

[6] Goto C, Ogawa Y. Numerical Method of Tsunami Simulation with the Leap-Frog Scheme, Report of Department of Civil Engineering. Faculty of Engineering, Tohoku University; 1982. p. 52 (in Japanese)

[7] Intergovernmental Oceanographic Commission. Numerical Method of Tsunami Simulation with the Leap-Frog Scheme (Manuals and Guides 35), IUGG/IOC TIME PROJECT, UNESCO. 1997; Part 1, Chapter 1, 1–19 http://tsunami190245.tripod.com/tsh.pdf (last accessed in April 30, 2018)

[8]   Imamura F, Yalcine A C, Ozyurt G. Tsunami Modelling Manual; April 2006. 58p. http://www.tsunami.civil.tohoku.ac.jp/hokusai3/J/projects/manual-ver-3.1.pdf (last accessed in April 30, 2018)

[9]   Goto K, Fujima K, Sugawara D, Fujino S, Imai K, Tsudaka R, Abe T, Haraguchi T. Field measurements and numerical modeling for the run-up heights and inundation distances of the 2011 Tohoku-oki tsunami at Sendai plain, Japan. Earth, Planets and Space. 2012;**64**: 1247-1257

[10] Oishi Y, Imamura F, Sugawara D. Near-field tsunami inundation forecast using the parallel TUNAMI-N2 model: Application to the 2011 Tohoku-Oki earthquake combined with source inversions. Geophysical Research Letters. 2015;**42**(4):1083-1091

[11] Tsushima H, Hirata K, Hayashi Y, Tanioka Y, Kimura K, Sakai S, Shinohara M, Kanazawa T, Hino R, Maeda K. Near-field tsunami forecasting using offshore tsunami data from the 2011 off the Pacific coast of Tohoku earthquake. Earth, Planets and Space. 2011;**63**:821-826

[12] Mansinha L, Smylie DE. The displacement fields of inclined faults. Bulletin of the Seismological Society of America. 1971;**61**:1433-1440

[13] Iwasaki T, Mano A. Two-Dimensional Numerical Simulation of Tsunami Run-ups in Eulerian Description, Proc. 26th Conference on Coastal Engineering, Japan Society of Civil Engineers; 1979. pp. 70-74 (in Japanese)

[14] Satake K, Nanayama F, Yamaki S. Source models of the unusual tsunami in the 17th century in eastern Hokkaido. Annual Report on Active Fault and Paleoearthquake Researches. 2003;**3**:315-362 (in Japanese)

[15] Japan Hydrographic Association. JTOPO30 (30-second grid water depth data in Japan's coastal waters http://www.mirc.jha.jp/products/finished/JTOPO30/ (in Japanese, last accessed in April 30, 2018)

[16] Japan Oceanographic Data Center, Japan Coast Guide. The coast 500 m grid water depth http://jdoss1.jodc.go.jp/vpage/depth500_file.html (last accessed in April 30, 2018)

[17] Geospatial Information Authority of Japan. The Land Altitude Data of 50 m Grid. https://fgd.gsi.go.jp/download/menu.php (in Japanese, last accessed in April 30, 2018)

[18] Si H, Midorikawa S. New relationship for peak acceleration and velocity considering effects of fault type and site condition. Journal of Structural and Construction Engineering, Architectural Institute of Japan. 1999;**523**:63-70 (in Japanese)

[19] Si H, Midorikawa S. New attenuation relations for peak ground acceleration and velocity considering effects of fault type and site condition, Proc. 12th World Conference on Earthquake Engineering. Paper No. 0532. 30 January - 4 February 2000; Auckland, New Zealand. 8p

[20] Midorikawa S, Ohtake Y. Variance of peak ground acceleration and velocity in attenuation relationships. Proc. 13th World Conference on Earthquake Engineering. Paper No. 325. 1-6 August 2004; Vancouver, Canada. 10p

[21] Honda R, Aoi S, Morikawa N, Sekiguchi H, Kunugi T, Fujiwara H. Ground motion and rupture process of the 2003 Tokachi-oki earthquake obtained from strong motion data of K-NET and KiK-net. Earth, Planets and Space. 2004;**56**:317-322

[22] Aoi S, Sekiguchi H, Morikawa N, Kunugi T. Source process of the 2007 Niigata-ken Chuetsu-oki earthquake derived from near-fault strong motion data. Earth, Planets and Space. 2008;**60**:1131-1135

[23] Aoi S, Kunugi T, Suzuki W, Morikawa N, Nakamura H, Senna S, Fujiwara H. Strong motion characteristics of the 2011 Tohoku-Oki earthquake. Zisin (Journal of Seismological Society of Japan). 2012;**64**:169-182 (in Japanese)

[24] Suzuki W, Aoi S, Kunugi T. Strong motions observed by KNET and KiK-net during the 2016 Kumamoto earthquake sequence, earth. Planets and Space. 2017;**69**:19, 12

[25] Fujimoto K, Midorikawa S. Empirical method for estimating J.M.A. Instrumental seismic intensity from ground motion parameters using strong motion records during recent major earthquakes. Journal of Social Safety Science. 2005;**7**:241-246 (in Japanese)

[26] Fujimoto K, Midorikawa S. Relationship between average shear-wave velocity and site amplification inferred from strong motion records at nearby station pairs. Journal of Japan Association for Earthquake Engineering. 2006;**6**:11-22 (in Japanese)

[27] Fujimoto K, Midorikawa S. Simplified method for predicting average shear-wave velocity of ground at strong-motion stations. Proc. 14th World Conference on Earthquake Engineering. Paper No. 02-0016; 12–17 October 2008; Beijing, China. 10p

[28] National Research Institute for Earth Science and Disaster Prevention. Japan Seismic Hazard Information Station (J-SHIS). http://www.j-shis.bosai.go.jp/ (last accessed in April 30, 2018)

[29] Wakamatsu K, Matsuoka M. Nationwide 7.5-arc-second Japan engineering geomorphologic classification map and Vs30 zoning. Journal of Disaster Research. 2013;**8**:90-911

[30] Matsuoka M, Wakamatsu M, Hashimoto M. Liquefaction potential estimation based on the 7.5-arc-second Japan engineering geomorphologic classification map. Journal of Japan Association for Earthquake Engineering. 2011;**1**:20-39 (in Japanese)

[31] Matsuoka M, Wakamatsu M, Hashimoto M, Senna S, Midorikawa. Evaluation of liquefaction potential for large areas based on geomorphologic classification. Earthquake Spectra. 2015;**31**:2375-2395

[32] Senna S, Hasegawa N, Maeda T, Fujiwara H. Liquefaction damage of the Tonegawa basin caused by the 2011 off the Pacific Coast of Tohoku Earthquake. Proc. International Symposium on Engineering Lessons Learned from the 2011 Great East Japan Earthquake. 1-4 March 2012; Tokyo, Japan. pp. 719-730